LISA science performance in observations of short-lived signals from massive black hole binary coalescences

Pratten, Geraint; Klein, Antoine; Moore, Christopher J.; Middleton, Hannah; Steinle, Nathan; Schmidt, Patricia; Vecchio, Alberto

DOI:
10.1103/PhysRevD.107.123026

LISA science performance in observations of short-lived signals from massive black hole binary coalescences

Geraint Pratten, Antoine Klein, Christopher J. Moore, Hannah Middleton, Nathan Steinle, Patricia Schmidt, and Alberto Vecchio

Institute for Gravitational Wave Astronomy and School of Physics and Astronomy, University of Birmingham, Birmingham B15 2TT, United Kingdom

(Received 8 December 2022; accepted 30 May 2023; published 22 June 2023)

The observation of massive black hole binary systems is one of the main science objectives of the Laser Interferometer Space Antenna (LISA). The instrument's design requirements have recently been revised: they set a requirement at 0.1 mHz, with no additional explicit requirements at lower frequencies. This has implications for observations of the short-lived signals produced by the coalescence of massive and high-redshift binaries. Here we consider the most pessimistic scenario: the (unlikely) case in which LISA has no sensitivity below 0.1 mHz. We show that the presence of higher multipoles (beyond the dominant $\ell = |m| = 2$ mode) in the gravitational radiation from these systems, which will be detectable with a total signal-to-noise ratio $\sim 10^3$, allows LISA to retain the capability to accurately measure the physical parameters and the redshift and to constrain the sky location. To illustrate this point, we consider a few select binaries in a total (redshifted) mass range of 4×10^6–$4 \times 10^7 M_\odot$ whose ($\ell = |m| = 2$) gravitational-wave signals last between $\approx$ 12 h and $\approx$20 days in band. We model the emitted gravitational radiation using the highly accurate (spin-aligned) waveform approximant IMRPhenomXHM and carry out a fully coherent Bayesian analysis on the LISA noise-orthogonal time-delay-interferometry channels.

DOI: 10.1103/PhysRevD.107.123026

I. INTRODUCTION

Reconstructing the merger history of massive ($\sim 10^7$–$10^5 M_\odot$) black holes (MBHs), understanding their hosts and how they (co)evolve over cosmic time, and determining their mass function and how it relates to the galaxies that harbor them are some of the most important open problems in astrophysics and cosmology, see, e.g., [1] and references therein for a review. The Laser Interferometer Space Antenna (LISA) [2], a gravitational-wave (GW) observatory that is currently being developed for science operation in the next decade, will provide major new observational capabilities to tackle these questions, see, e.g., [3] and references therein. The results of this first GW survey capable of discovering MBH binaries throughout the Universe, complemented by a slew of other surveys and GW-triggered observations, e.g., in optical (LSST [4]), mm/radio (ALMA [5]/SKA [6]), near infrared (James Webb Space Telescope [7]), and X-ray (e.g., Athena [8]), is likely to provide a significant leap forward in our understanding of the formation and evolution of entire populations of MBHs.

LISA will observe the last hours to years of the lifetimes of MBH binaries. Observationally, the MBH binary merger rate is de facto unconstrained. Theoretical models predict wildly different rates depending on the assumptions, see, e.g., [9]. As a consequence, the expected number of LISA detections varies from $\mathcal{O}(1)$ to $\mathcal{O}(100)$ per year with a mission lifetime of 4.5 years and a possible extension of up to 10 years. While there are numerous physical mechanisms that determine the population properties of massive black hole binaries (MBHBs), the seed prescription is a source of crucial uncertainty and plays a key role in setting the MBHB mass distribution. The light-seed scenario assumes that BHs first form at high redshifts $z \sim 15$–20 and at comparatively low masses $\sim [10^2, 10^3] M_\odot$ from the collapse of heavy population III stars that form in low-metallicity environments, e.g., [1,10–12]. In contrast, the heavy-seed scenario assumes thats BHs already form with large masses $\sim [10^4, 10^5] M_\odot$ at high redshift $z \sim 15$–20, e.g., through the collapse of a protogalactic disk [1,12–14]. Regardless of the details of the model, the general trend is that one expects a handful of massive binaries ($> 10^6 M_\odot$), as these constitute the bulk of the currently observed MBH population [15–17]. In such a scenario, the detection of MBHs would be rare and from massive systems. If, however, comparably lighter MBHs are present, then the event rate could reach hundreds of binaries.

The low-frequency sensitivity of LISA plays a vital role in determining the instrument's capability for detecting and characterizing MBH binaries. In particular, it enters the analysis in two crucial ways that collectively determines the LISA science performance for the MBH parameter space.

First, it sets the maximum mass and redshift of the binaries that can be observed. For reference, the frequency of the innermost stable circular orbit (ISCO) associated with the dominant $\ell = |m| = 2$ mode of gravitational radiation for a quasicircular binary of nonspinning MBHs with individual (source-frame) masses[1] $m_{1,2}^{(\mathrm{src})}$ and total mass $M^{(\mathrm{src})} = m_1^{(\mathrm{src})} + m_2^{(\mathrm{src})}$ at redshift z is approximately

$$f_{\mathrm{ISCO}}^{(2,2)} \sim 0.4 \left[\frac{M^{(\mathrm{src})}(1+z)}{10^7 M_\odot}\right]^{-1} \mathrm{mHz}. \quad (1)$$

Similarly, the frequency of the dominant quasinormal mode of the remnant black hole produced in a merger as it settles to a quiescent state is approximately

$$f_{\mathrm{ring}}^{(2,2)} \sim 3.2 \left[\frac{M^{(\mathrm{src})}(1+z)}{10^7 M_\odot}\right]^{-1} \mathrm{mHz}. \quad (2)$$

These frequencies obey a natural hierarchy $f_{\mathrm{ring}} > f_{\mathrm{ISCO}}$, such that for a given instrument low-frequency cutoff f_{low} there is a regime in which the mass and redshift of the binary are sufficiently high that the GW signal is pushed out of band, rendering the binary unobservable.

Second, the low-frequency cutoff determines how long the signal will be in the detection band. The leading-order post-Newtonian duration of the ($\ell = |m| = 2$) signal from a binary in the LISA band can be written as

$$\tau \sim \left(\frac{3}{4\eta}\right)\left(\frac{f_{\mathrm{low}}}{0.1\ \mathrm{mHz}}\right)^{-8/3}\left[\frac{M^{(\mathrm{src})}(1+z)}{10^7 M_\odot}\right]^{-5/3} \mathrm{days}, \quad (3)$$

where $\eta = m_1 m_2/M^2$ is the symmetric mass ratio. The number of GW cycles in band scales as $N \sim \tau f_{\mathrm{low}}$, meaning that a shorter time in band will reduce our ability to accurately measure the physical parameters of the binary. In addition, this timescale has to be compared to $T_{\mathrm{LISA}} = 1$ yr, the time taken for the constellation to orbit the Sun and precess around the perpendicular to the ecliptic. The combination of these motions induces sky-location-dependent modulations in the observed GW signal, providing the angular resolution of the LISA observatory. If $\tau \ll T_{\mathrm{LISA}}$, the observatory cannot resolve the source position in the sky, unless sky-location-dependent information is encoded in the gravitational-wave polarization amplitudes.

A recent important development in the mission design is to impose a requirement at 0.1 mHz, but no explicit sensitivity requirement below this frequency [18,19]. One may therefore wonder what would be the impact of the (unlikely) case in which sensitivity is lost below $f_{\mathrm{low}} = 0.1$ mHz. This means that, as well as losing sensitivity to some of the most massive systems, reduced duration of MBHB signals in band impacts the science performance of the mission, particularly the ability to locate a source in the sky, which depends on the motion of the constellation as the coalescence takes place.

Many studies have been carried out over the years to explore LISA performance in observations of MBHBs, using different assumptions and/or approximations, see, e.g., [12,20–26] and references therein. However, all these studies assumed a detection bandwidth that extended below 0.1 mHz.

In this paper, we take a worst case scenario approach concerning the impact of the new low-frequency design requirements and consider the most pessimistic circumstance in which LISA has no sensitivity below $f_{\mathrm{low}} = 0.1$ mHz. We explore the concomitant impact on the science capability of LISA in observing MBHBs by considering a small number of high-mass systems over a total (redshifted) mass range $4 \times 10^6 M_\odot$–$4 \times 10^7 M_\odot$. These systems produce short-lived coalescences, such that the dominant $\ell = |m| = 2$ harmonic is in the LISA band for ≈ 12 h for the heaviest binary through to ≈ 3 weeks for the lightest. We use a fully Bayesian analysis framework on the three time-delay-interferometry (TDI) LISA observables to compute the posterior probability density functions (PDFs) of the source parameters. The gravitational-wave signal is modeled using the IMRPhenomXHM approximant, which is extremely accurate for binaries with a mass ratio $q = m_2/m_1 > 1/20$ and for BHs with spins (anti)aligned with the orbital angular momentum. The IMRPhenomXHM model, incorporates higher multipoles (HM) beyond the dominant (2,2) mode.

We demonstrate that LISA retains excellent performance in measuring the masses, spins, redshift [assuming a fixed Λ cold dark matter (ΛCDM) cosmology], and sky localization of MBH binaries. For lighter MBHBs, as predicted in light-seed scenarios, changes to the low-frequency cutoff have a minimal impact on our ability to characterize their astrophysical properties. Importantly, for the heavier MBHBs predicted in heavy-seed scenarios, we find only a small loss of performance in our ability to characterize their astrophysical source properties. This is due to the fact that these binaries will be observed with total SNRs $\sim 10^3$ and that multipoles beyond the dominant (2, 2) mode in the gravitational-wave strain will be detectable with SNRs $\sim$ 1–100. The higher multipoles provide location-dependent information that is intrinsic

[1]Throughout the paper we adopt the convention that mass parameters in the source frame are labeled by the suffix "src," so that the redshifted mass parameter m is related to its source-frame value by $m^{(\mathrm{src})}$, by $m = m^{(\mathrm{src})}(1+z)$, where z is the redshift.

to the gravitational-wave signal emitted by the binary and does not rely on the instrument's motion. In addition, the presence of higher multipoles also reduces correlations across many parameters, in agreement with [22–32].

The paper is organized as follows: in Sec. II we describe the method and assumptions used in this work. Section III presents the main results, with further details provided in the Appendix. Section IV contains our conclusions and highlights future work.

II. METHOD

Our goal is to explore the accuracy to which the parameters $\boldsymbol{\theta}$, which describe a MBHB, can be measured by LISA. In order to do this, we compute the posterior PDF,

$$p(\boldsymbol{\theta}|d) \propto \mathcal{L}(d|\boldsymbol{\theta})p(\boldsymbol{\theta}), \tag{4}$$

given the data d. In the above expression, $\mathcal{L}(d|\boldsymbol{\theta})$ is the likelihood, and $p(\boldsymbol{\theta})$ is the prior, which we describe below.

We employ a coherent analysis using the three noise-orthogonal TDI channels $\{A, E, T\}$, which constitute the data d in Eq. (4) and are synthesized from the LISA phase meters [33]. The LISA response is modeled following the rigid adiabatic approximation, e.g., Ref. [34], implying that we are working with TDI variables of generation 1.5. The actual analysis of the data will require a more sophisticated TDI scheme to suppress the laser frequency noise, but for the purpose of this paper, the approximation does not affect the core results. The likelihood in Eq. (4) can be written as [27]

$$\ln \mathcal{L}(d|\boldsymbol{\theta}) = -\sum_k \frac{\langle d_k - h_k(\boldsymbol{\theta})|d_k - h_k(\boldsymbol{\theta})\rangle_k}{2} + \text{const}, \tag{5}$$

where the sum is taken over the three TDI channels, labeled by k, and h_k denotes the TDI signal produced by a MBH binary with source parameters $\boldsymbol{\theta}$. The noise-weighted inner product is defined in the usual way

$$\langle a|b\rangle_k = 2\int_{f_{\rm low}}^{f_{\rm high}(\boldsymbol{\theta})} \frac{\tilde{a}(f)\tilde{b}^*(f) + \tilde{a}^*(f)\tilde{b}(f)}{S_k(f)}\mathrm{d}f. \tag{6}$$

In the above equation, $\tilde{a}(f)$ denotes the Fourier transform of the time series $a(t)$, $S_k(f)$ is the noise power spectral density of the kth TDI channel, and $f_{\rm low} = 0.1$ mHz is LISA's low-frequency cutoff. The highest frequency of the signal produced by a MBH binary $f_{\rm high}(\boldsymbol{\theta})$ depends on the source parameters. We use noise spectral densities $S_k(f)$ as given in European Space Agency's Science Requirements Document [18,19], with the important addition of a hard low-frequency cutoff $f_{\rm low}$ at 0.1 mHz. The unresolved Galactic confusion noise is modeled according to the analytical fit given in [35].

For the computation of the gravitational-wave polarizations $h_{+,\times}$, we assume that, regardless of formation history, the binaries circularize by the time they enter the LISA sensitivity band due to radiation reaction, e.g., [36]. We use IMRPhenomXHM [37,38] to model the full coalescence of quasicircular binaries, i.e., the inspiral, merger, and ringdown. The aligned-spin modes $h_{\ell m}$ are calibrated to numerical relativity and include the $(\ell, |m|) = \{(2,2),(2,1),(3,3),(3,2),(4,4)\}$ multipoles. In this study, we only consider aligned-spin binaries, i.e., systems in which the MBH spins are parallel or antiparallel to the orbital angular momentum. Spins that are misaligned with the orbital angular momenta, which induces precession of the orbital plane and the spins themselves, are not considered in this study, though we will return to them in a future study.

With these assumptions, the signal parameter set $\boldsymbol{\theta}$ consists of two independent mass parameters, e.g., the (redshifted) chirp mass $\mathcal{M}_c$ and mass ratio $q \equiv m_2/m_1 \leq 1$, the dimensionless spins, $\chi_i \equiv \vec{S}_{1,2}\cdot\hat{L}/m_{1,2}^2$, where $\vec{S}_i$ is the intrinsic spin angular momenta of the BH and $\hat{L}$ is the (constant) orbital angular momentum unit vector, the location of the source in the sky, in terms of the ecliptic latitude b and longitude l, the luminosity distance of the source $d_L(z)$, or equivalently, the redshift z (we assume standard ΛCDM cosmology according to Planck 2018 [39]), two parameters that describe $\hat{L}$, taken to be the inclination angle ι with respect to the line of sight and the GW polarization phase ψ, and, finally, the coalescence time t_c and associated GW phase ϕ_c. Note that t_c and ϕ_c correspond to a gauge freedom and are defined with respect to an arbitrary reference value.

To perform all parameter estimation, we use BALROG, a software package under development for LISA data analysis, see, e.g., [40–43]. We perform full Bayesian inference on simulated data using the nested sampling [44] algorithm implemented in DYNESTY [45] to evaluate Eq. (4). All injections are performed in zero noise.

III. RESULTS

We consider a small number of representative systems for this study. The key source parameters are listed in Table I and are chosen to be broadly consistent with predictions from theoretical models, see, e.g., [3,12,46] and references therein. We focus on binaries, whose combination of masses and redshift are mostly affected by the new low-frequency design requirement, and consider four MBHBs with redshifted total mass in the range $4\times10^6 M_\odot$–$4\times10^7 M_\odot$ (with $z = 3$ in all cases). For all the systems, we set the mass ratio to $q = 1/4$ and the (aligned) spins to moderate values, $\chi_1 = 0.4$ and $\chi_1 = 0.2$, corresponding to an effective aligned spin $\chi_{\rm eff} = 0.24$, where [47–49]

$$\chi_{\rm eff} = \frac{(m_1\vec{\chi}_1 + m_2\vec{\chi}_2)\cdot\vec{L}_N}{M}. \tag{7}$$

TABLE I. Main properties of the injected sources and the recovered parameters. The injection values are denoted with the subscript "inj." The second column (HM) shows whether the injection and recovery are done including all the available modes in the waveform approximant (denoted with ✓) or just the (2, 2) mode (denoted with ✗). We stress that the approximant used in the injection and the likelihood are identical. The masses in the table are the redshifted masses and the injected spins are $\chi_1 = 0.4$ and $\chi_2 = 0.2$. The redshift for all binaries is $z = 3$. For the recovered parameters, we show the median posterior value and the 90% probability interval. Ω_{90} is the 90% probability interval of the 2D source location in the sky injection and t_c is the time of coalescence with respect to an arbitrary reference epoch (the same applies to the phase of coalescence). The extrinsic parameters that are not reported in the table were the same for all the sources, with the following values: ecliptic longitude $l = 2.0$ and latitude $\sin b = 0.3$, inclination angle $\cos \iota = 0.9$, and polarization $\psi = 0.4$ (the time and phase at coalescence are subject to an arbitrary choice of their zero value, therefore we do not report them here). The binaries marked with a ⋆ indicate that the posteriors for Ω_{90} and Δt_c are multimodal (MM) and that due caution should be used in interpreting these numbers.

ID	HM	$m_1^{\rm inj}$ ($10^6 M_\odot$)	$m_2^{\rm inj}$ ($10^6 M_\odot$)	$f_{\rm low}$ (mHz)	SNR	$\tau_{(\ell=2)}$ (days)	$\tau_{(\ell=3)}$ (days)	$\tau_{(\ell=4)}$ (days)	m_1 ($10^6 M_\odot$)	m_2 ($10^6 M_\odot$)	z	Ω_{90} (deg^2)	Δt_c (s)	MM
I	✓	32.0	8.0	0.1	486	0.46	1.15	2.63	$32.01^{+0.12}_{-0.14}$	$8.00^{+0.24}_{-0.21}$	$3.01^{+0.07}_{-0.07}$	5.9	12.3^{+605}_{-246}	⋆
Ia	✓	32.0	8.0	0.05	501	2.95	8.29	18.4	$32.00^{+0.12}_{-0.12}$	$8.02^{+0.12}_{-0.13}$	$3.02^{+0.05}_{-0.04}$	4.2	8.2^{+436}_{-238}	⋆
Ib	✓	32.0	8.0	0.01	505	215	654	1409	$32.00^{+0.15}_{-0.15}$	$8.01^{+0.09}_{-0.09}$	$3.00^{+0.03}_{-0.03}$	0.8	$-0.6^{+28.8}_{-28.6}$	
I	✗	32.0	8.0	0.1	453	0.46	⋯	⋯	$32.02^{+0.62}_{-0.54}$	$8.01^{+0.63}_{-0.80}$	$2.66^{+0.54}_{-0.58}$	3461	-38^{+713}_{-262}	⋆
II	✓	16.0	4.0	0.1	638	1.31	4.35	9.36	$16.00^{+0.05}_{-0.05}$	$4.00^{+0.03}_{-0.03}$	$3.00^{+0.03}_{-0.02}$	1.0	1.5^{+425}_{-10}	⋆
II	✗	16.0	4.0	0.1	593	1.31	⋯	⋯	$16.03^{+0.13}_{-0.13}$	$3.98^{+0.09}_{-0.07}$	$2.60^{+0.45}_{-0.62}$	244	336^{+136}_{-488}	⋆
III	✓	6.4	1.6	0.1	1078	6.80	20.0	43.1	$6.40^{+0.01}_{-0.01}$	$1.60^{+0.004}_{-0.004}$	$3.00^{+0.01}_{-0.01}$	0.2	$0.45^{+3.50}_{-2.64}$	
III	✗	6.4	1.6	0.1	849	6.80	⋯	⋯	$6.40^{+0.02}_{-0.02}$	$1.60^{+0.005}_{-0.007}$	$3.03^{+0.17}_{-0.43}$	17.8	$0.4^{+6.5}_{-31.3}$	
IV	✓	3.2	0.8	0.1	1706	22.1	63.6	137	$3.20^{+0.007}_{-0.007}$	$0.80^{+0.002}_{-0.002}$	$3.002^{+0.007}_{-0.007}$	0.08	$0.00^{+1.12}_{-1.14}$	
IV	✗	3.2	0.8	0.1	1693	22.1	⋯	⋯	$3.20^{+0.005}_{-0.005}$	$0.80^{+0.002}_{-0.001}$	$2.84^{+0.31}_{-0.21}$	13.8	$0.05^{+8.2}_{-16.9}$	

As shown in Table I, for all these binaries the time spent in band by the dominant $\ell = |m| = 2$ mode of the gravitational radiation is much shorter than $T_{\rm LISA}$: it ranges from ≈ 0.5 days (for $M = 4 \times 10^7 M_\odot$) to ≈ 22 days (for $M = 4 \times 10^6 M_\odot$). However, gravitational radiation from higher ($\ell = 3$ and 4) multipoles is within the observational band for longer periods, with radiation from each multipole ℓ in the sensitivity band for a time $\tau_\ell = \tau(\ell/2)^{8/3}$, where τ is approximated by Eq. (3). They range from ≈ 3 days for $M = 4 \times 10^7 M_\odot$ through to ≈ 137 days for $M = 4 \times 10^6 M_\odot$.

The higher multipoles also contribute a factor of a few through to several tens to the total SNR of the binary depending on the specific source parameters.

For each of the four choices of total mass (labeled ID in Table I), we generate synthetic data in which we set $f_{\rm low} = 0.1$ mHz and inject and recover the coalescence signal using only the (2, 2) mode and the full set of modes available in the approximant IMRPhenomXHM (denoted with ✗ and ✓, respectively, in column HM of Table I). We stress that, for each of the runs, the injection and recovery is done with an *identical* waveform model, as we want to explore the impact of the higher multipoles on the analysis and not to concern ourselves with parameter biases arising from systematic errors between waveform approximants. The total signal-to-noise ratio produced by these binaries is in the range $\approx 6 \times 10^2$–2×10^3.

To provide a quantitative assessment of the impact on the LISA science performance imposed by the new low-frequency design requirement, we repeat the analysis for the heaviest binary (ID I in Table I), $m_1 = 3.2 \times 10^7 M_\odot$ and $m_2 = 8 \times 10^6 M_\odot$, using a range of low-frequency cutoffs, i.e., $f_{\rm low} = 0.05$ mHz (Ia) and $f_{\rm low} = 0.01$ mHz (Ib).

The results are summarized in Table I, and Figs. 1(a)–1(d) show the 2D PDFs for selected parameters of interest for each of the MBH binaries. We also compare the results obtained by considering only the (2, 2) mode against those obtained using the full range of higher multipoles available. Full corner plots are provided in Figs. 3–6 of the Appendix. In Fig. 2 we compare the posterior PDFs on selected parameters obtained by assuming different low-frequency cutoffs for the heaviest system, to provide a quantitative indication of the impact of the new design requirements.

The first general trend observed is that one draws radically different conclusions on the LISA science performance, described by the size of the statistical errors on the system parameters, if one considers only the dominant (2, 2) mode [green contours in Figs. 1(a)–1(d)] or if one includes the full set of higher multipoles, confirming results in other portions of the LISA parameter space [22–25]. For the binaries considered here, the 90% confidence intervals are typically larger by a factor ∼10–1000 for the (2, 2) mode results with respect to the full multipolar results. The

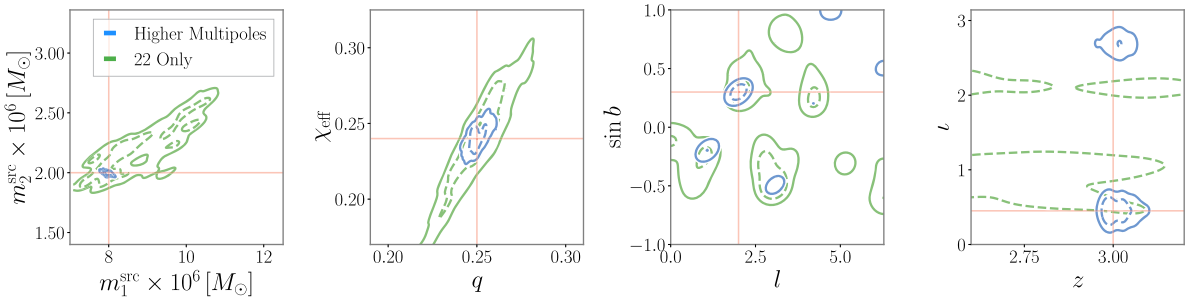

(a)

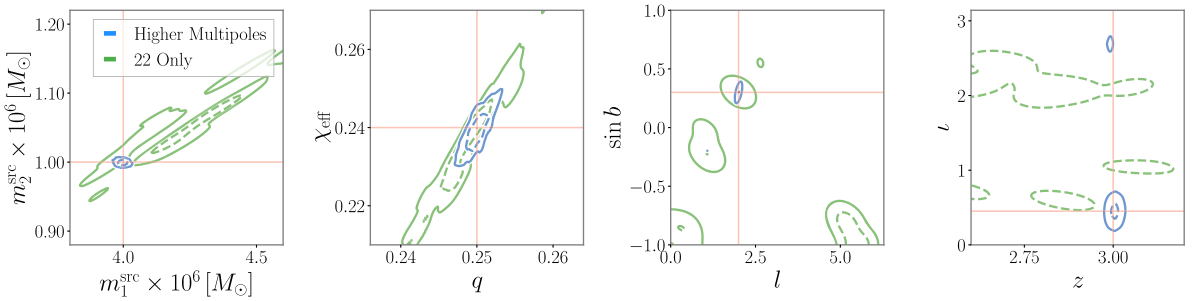

(b)

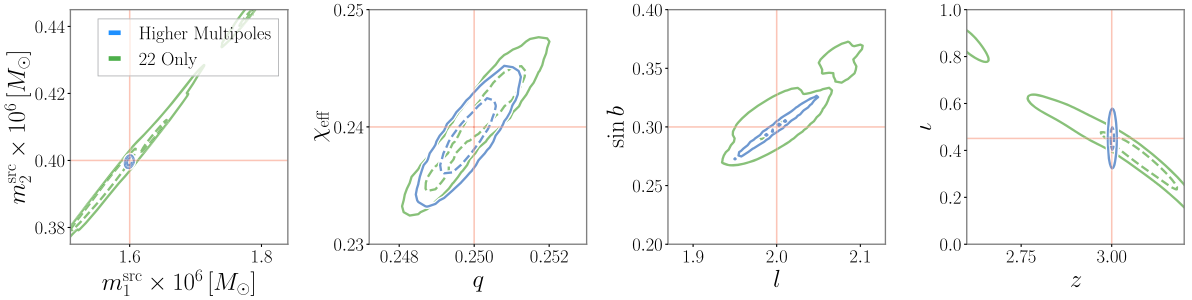

(c)

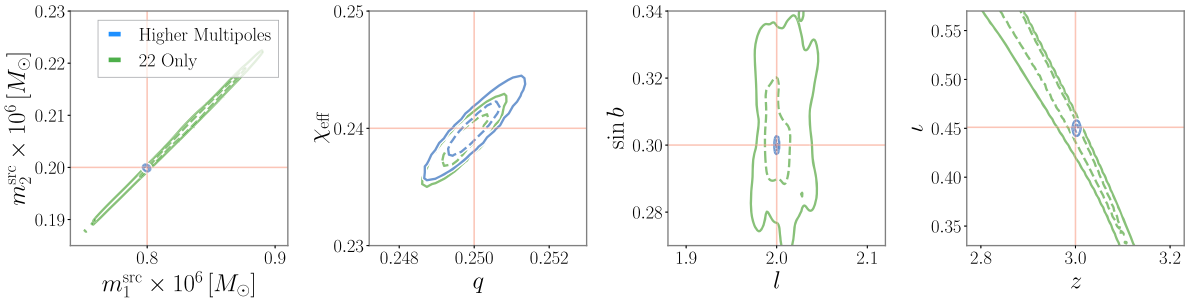

(d)

FIG. 1. Marginalized posterior density functions for selected parameters for the four systems of Table I, with $f_{\rm low} = 0.1$ mHz. (a) Systems ID I, (b) II, (c), III, and (IV), see corner plots in Figs. 3–6, respectively. The plots show the 50% (dashed) and 90% (solid) probability contours inferred when using higher multipoles (blue) and just the (2, 2) mode (green). The solid red lines denote the injection values.

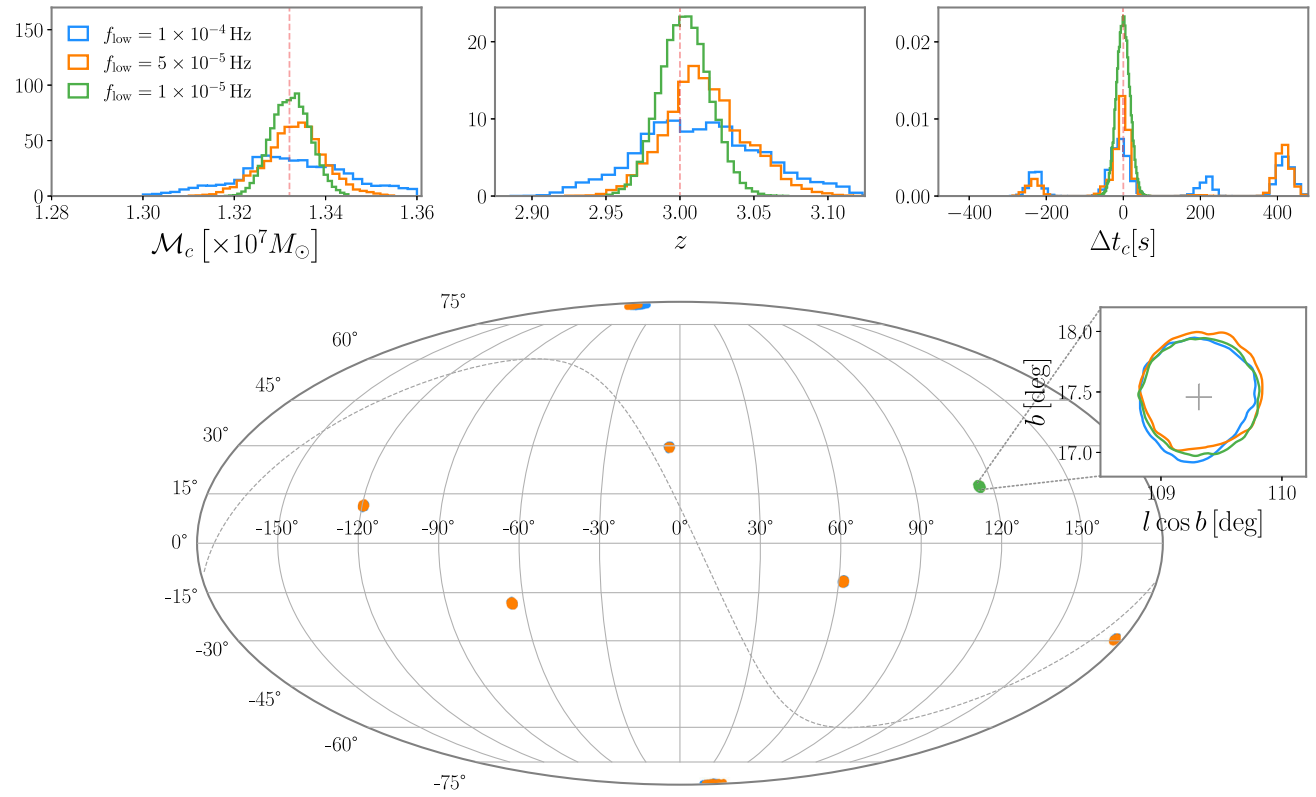

FIG. 2. Impact of lowering the cutoff frequency for the LISA sensitivity band $f_{\rm low}$ on the inferred parameters of a binary back hole with $m_1 = 3.2 \times 10^7 M_\odot$ and $m_1 = 8 \times 10^6 M_\odot$ (run ID: I, Ia, and Ib in Table I). Decreasing the cutoff frequency effectively means a longer duration signal within LISA's sensitive band, typically resulting in parameter degeneracies being broken due to the amplitude and phase modulations induced by LISA's orbital motion. Waveform models incorporating higher multipoles can partially mitigate against such changes due to the dependence of the multipoles on the binary geometry, i.e., its sky location and orientation. The coalescence time t_c is defined at the Solar System barycenter; therefore, different possible sky posteriors translate into different possible coalescence times. For $f_{\rm low} = 1 \times 10^{-4}$ and 5×10^{-5} Hz, we find eight modes, whereas for $f_{\rm low} = 1 \times 10^{-5}$ Hz, these degeneracies are broken and we find only one mode.

inclusion of higher multipoles has a strong impact on the correlations and degeneracies between parameters. Below, we focus on discussing the results obtained when using only the full set of modes.

We start by discussing the results on the physical parameters, i.e., the masses and spins. For the latter, we focus on the effective spin parameter $\chi_{\rm eff}$, as defined in Eq. (7), given its relevance for aligned-spin waveforms.

LISA retains excellent capability, by most astronomical standards, to measure the *individual* source-frame masses (assuming ΛCDM standard cosmology), which can be measured to $\approx 1\%$ (or better) for MBHBs within the parameter range considered here. This comes from the combination of the measurement of the detector-frame masses and the redshift (for the latter, see below). In fact, to understand the difference between the measurements of detector- vs source-frame masses, it is useful to compare the results of Figs. 1(a)–1(d), where we plot source-frame masses, with those of Table I, where we report results for detector-frame masses.

LISA equally maintains good capability to measure the effective spin parameter $\chi_{\rm eff}$, which is always measured with an error (at 90% credibility) ≈ 0.1–0.01. Due to the signatures of higher multipoles, the correlation between $\chi_{\rm eff}$ and the mass ratio q is largely broken, see Figs. 1(a)–1(d), even for signals that span a very short period in the LISA sensitivity band. The general trend is that the error on $\chi_{\rm eff}$ decreases as the number of wave cycles increases, therefore it is smaller for the lighter binaries considered here, which also happen to have the larger SNRs, see also [50–54].

We now turn our attention to the parameters that describe the time, distance, and sky localization of the MBHB merger. Accurately measuring these parameters will be critical in identifying the host galaxies (and/or galaxy clusters) of MBHB mergers and hence our ability to probe their environments through dedicated observational campaigns in the electromagnetic (EM) spectrum across many wavelengths [21,25,55]. Joint GW-EM observations will provide a wealth of information on the demographics, accretion processes, and high-energy radiative physics that

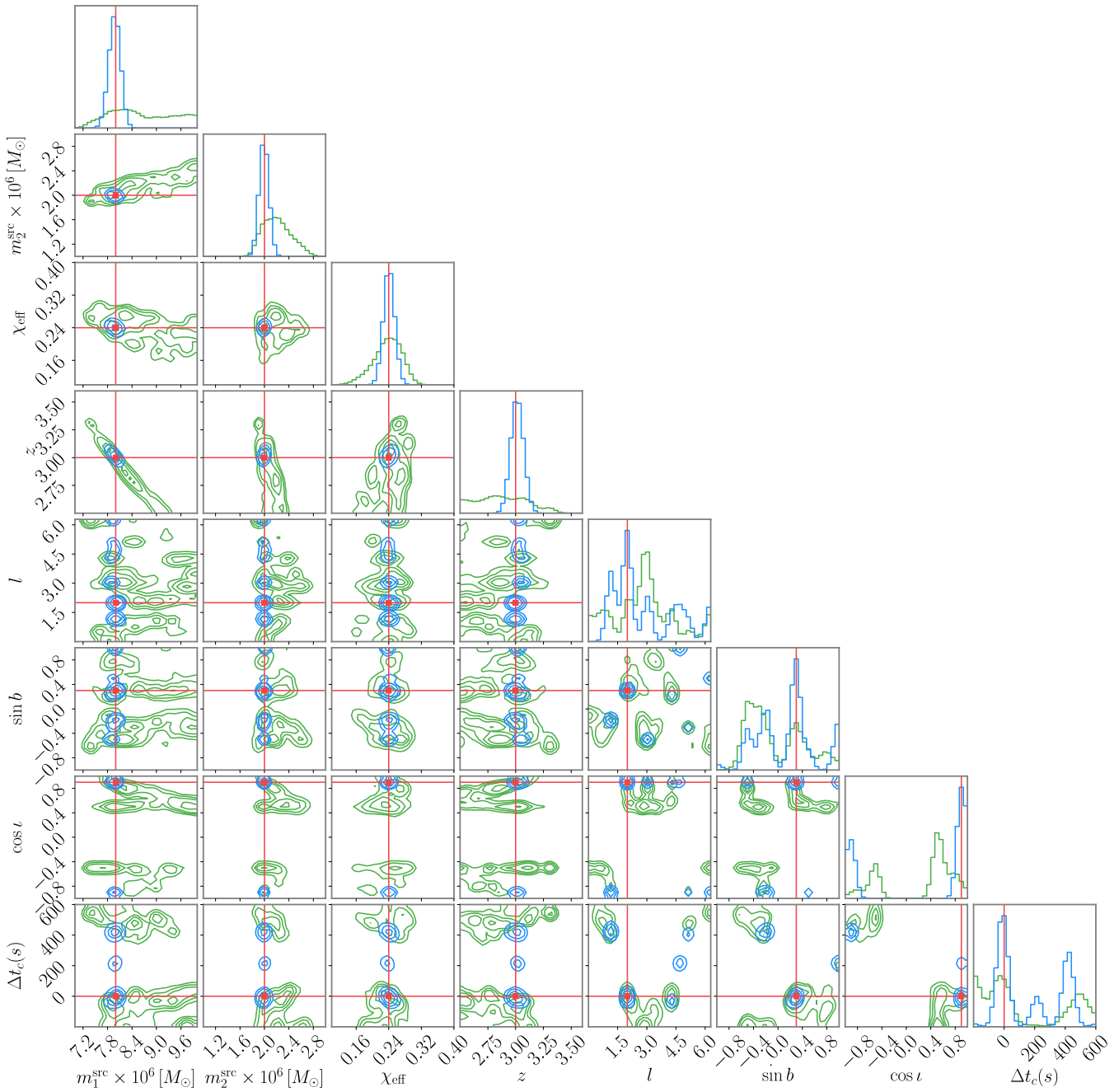

FIG. 3. Binary I. Run with higher multipoles (blue) and with the (2, 2) mode only (green). The red lines denote the injected values.

drives the merger of MBHBs throughout the Universe and allow us to probe their complete merger history across cosmic time [21,25,55]. If the local environment around the binary is gas rich, an EM counterpart could be generated through the accretion of gas onto the binary during the inspiral, merger, or ringdown. However, discriminating between these phases can provide important insight on astrophysical processes. For example, [56,57] discuss mechanisms producing EM features postmerger, whereas [58] argues that a disappearing thermal x-ray emission will be a characteristic signature of MBHB mergers, regardless of any postmerger effects. It is therefore useful to explore our ability to accurately localize the merger time for the MBHBs considered here.

The redshift determination, which comes from the direct measurement of the luminosity distance assuming a standard cosmology, is constrained to $z_{\rm inj} \pm 0.1$ for all the binaries considered here, where all systems have a fixed redshift $z = 3$. This comes from a combination of the comparatively high SNR, an accurate measurement of the

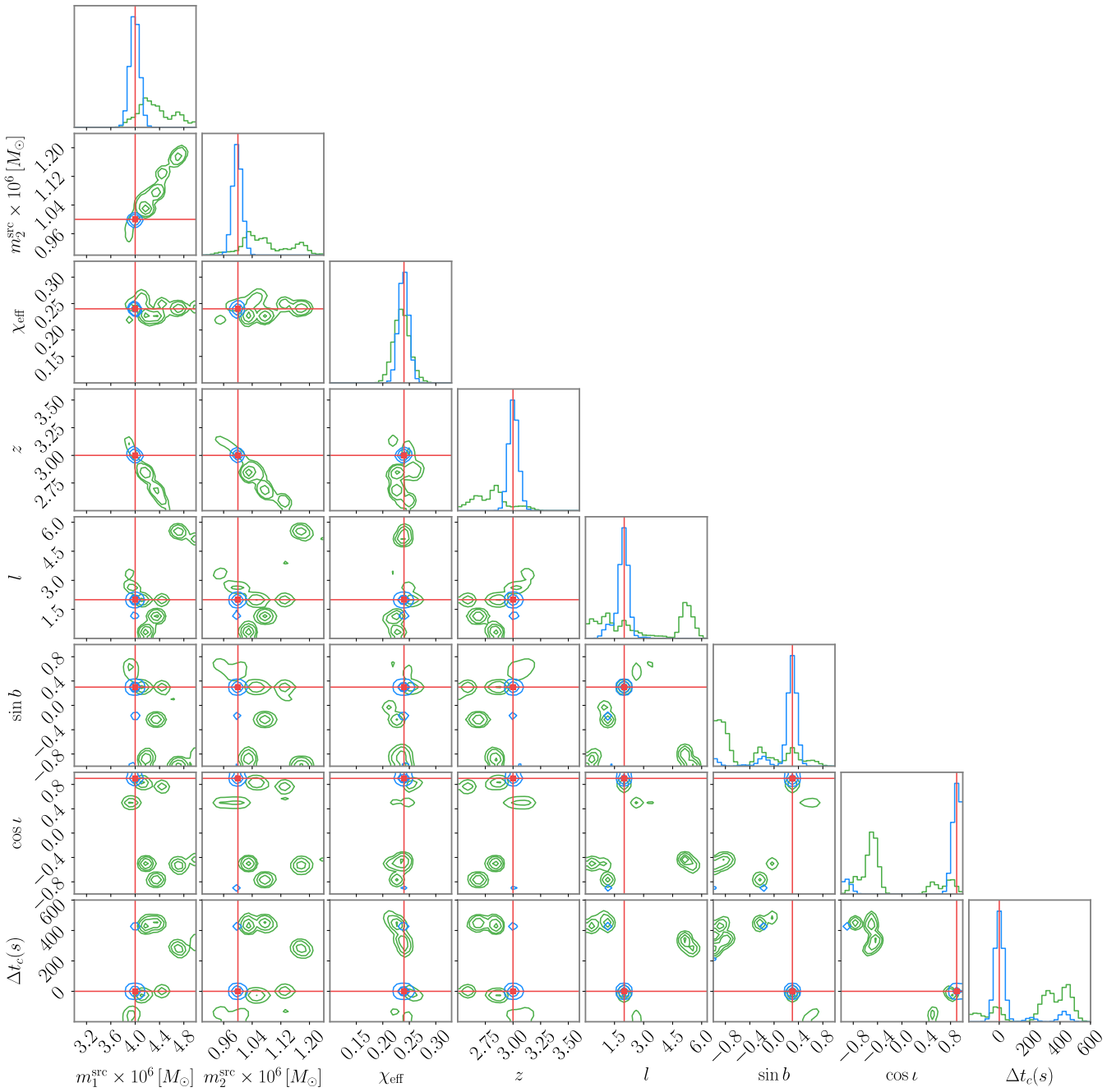

FIG. 4. Binary II. Run with higher multipoles (blue) and with the (2, 2) mode only (green). The red lines denote the injected values.

chirp mass, and the fact that the higher modes break correlations between parameters, in particular, the degeneracy between the distance and the inclination angle [27,59–63]. The redshifts are measured with a 90% credible interval of $\Delta z \approx 0.1$ for the heaviest binary ($M = 4 \times 10^7 M_\odot$) through to $\Delta z \approx 0.01$ for the lightest ($M = 4 \times 10^6 M_\odot$).

One may expect that it would be impossible for LISA to identify the source location in the sky, due to the signals being in band for a time $\ll T_{\rm LISA}$. However, higher multipoles, which also encode information about the source geometry, play a particularly important role. To estimate the sky area, we use a kernel density estimator provided by the LIGO.SKYMAP package [64–66]. For the shortest of the signals considered here, the dominant $\ell = |m| = 2$ mode is in band for half a day and the resulting 2D posterior PDF on the sky location is multimodal, albeit with well-constrained modes, whose local 90% probability regions are ~ 1 deg^2. By the time the $\ell = |m| = 2$ mode is in band for ≈ 1 week (for binary III,

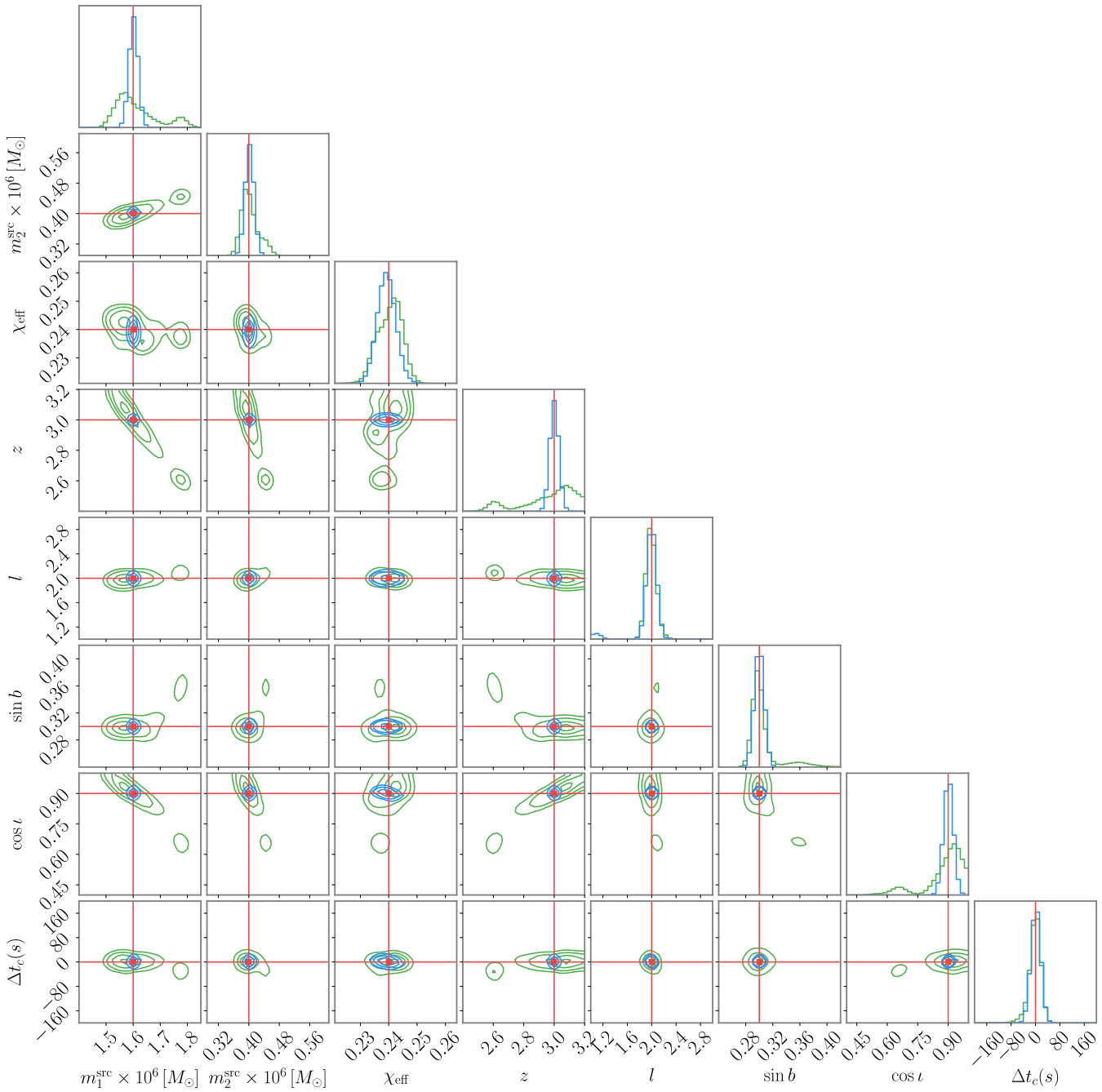

FIG. 5. Binary III. Run with higher multipoles (blue) and with the (2, 2) mode only (green). The red lines denote the injected values.

the $\ell = 3$ and $\ell = 4$ multipoles are in band for 20 and 43 days, respectively), the binary location is well constrained to a single mode with 90% probability interval, $\Omega_{90} \approx 1$ deg^2. As the mass of the binary decreases and the inspiral time goes up, the angular resolution increases accordingly. We note that the sky positions used here are defined in the Solar System barycenter, though recent work has introduced a new detector frame, the LISA frame, that would be more suited to the analysis of short-lived signals [22]. We do not explore the impact of such frame choices in this work.

The determination of the merger time is also affected by the multimodality of the sky location. For the shortest of the signals, there are multiple well-localized merger times that span an overall window of ≈ 10 min. As the number of cycles in band increases, the multimodality disappears. For the

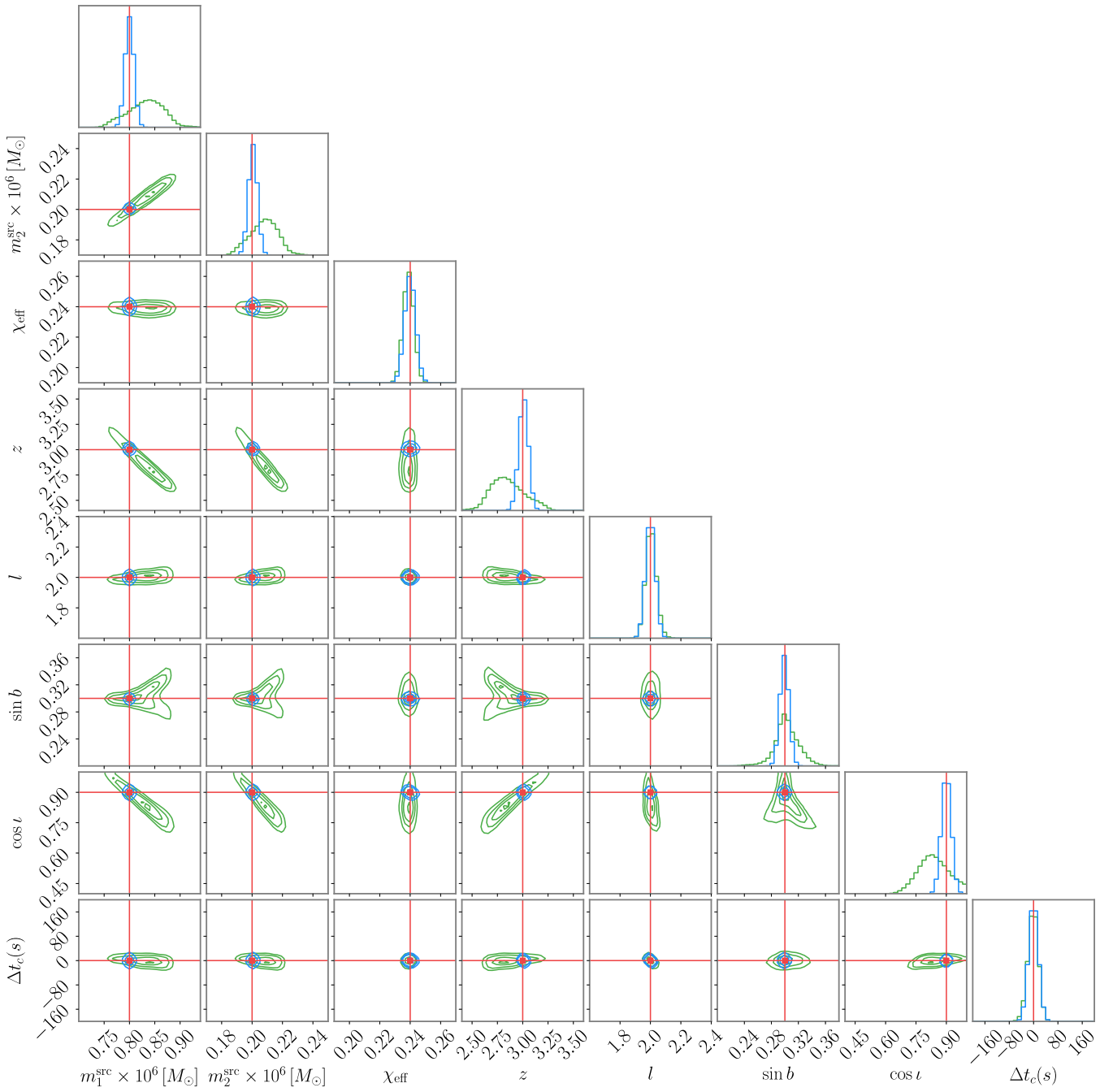

FIG. 6. Binary IV. Run with higher multipoles (blue) and with the (2, 2) mode only (green). The red lines denote the injected values.

lightest binary considered here, the merger time is measured to within a 90% confidence error of approximately 1 sec.

IV. CONCLUSIONS

We have explored the LISA science performance for observations of short-lived, high-redshift MBH binaries in light of the new low-frequency LISA design requirement that does not explicitly stipulate any sensitivity at frequencies below 0.1 mHz. We have considered a small number of binary parameters such that the signal is visible in band from 0.1 mHz through to merger and for a time significantly shorter than $T_{\rm LISA}$.

The results of this study can be taken as an indication that LISA would preserve its core science capabilities, despite some loss of performance, for short-lived signals, even if 0.1 mHz is a hard, low-frequency cutoff. However, this work should not be regarded as a detailed characterization of the expected LISA science performance: statistical errors that characterize the measurement accuracy

often strongly depend on the true binary parameters. Hence, a characterization of the science performance would require a large, and computationally costly, Bayesian inference campaign that goes beyond the scope of this paper.

As a corollary of this work, we have shown that including only the dominant $\ell = |m| = 2$ modes results in forecasting the accuracy of parameter determination which is worse by a factor ∼10–1000 for the very short-lived signals considered here, depending on the specific parameter under consideration and the binary parameters. It is well known that higher modes play an important role in LISA observations for MBHBs that produce SNRs $\sim 10^2$–10^3; however, the few studies carried out so far [22,24–26,67] have mainly considered lighter binaries that are observable for months to years and/or used a low-frequency cutoff ≈ 0.01 mHz, which radically change the observation.

Various assumptions made in this work should be relaxed in the future in the context of further systematic studies. Our assumption of aligned-spin systems has been driven by computational efficiency and is not necessarily supported by astrophysical expectations, see, e.g., [68,69] and reference therein. If spins are misaligned with respect to the orbital plane, additional phase and amplitude modulations induced by precession [70,71] will couple to LISA's ability to extract essentially the whole set of parameters of a binary and may actually *improve* LISA measurements [72,73]. We have also assumed that the power spectral density of the noise is known. This is not going to be the case for real observations, and accounting for additional elements of uncertainty, including data gaps, nonstationary noise, and transient instrumental glitches, will be required for more realistic predictions [74–76].

ACKNOWLEDGMENTS

We thank Antoine Petiteau for useful discussions. G. P. is grateful for support from a Royal Society University Research Fellowship URF\R1\221500 and RF\ERE \221015, and STFC Grant No. ST/V005677/1. A. K., H. M., C. J. M., and A. V. acknowledge the support of the UK Space Agency, Grants No. ST/V002813/1 and No. ST/X002071/1. N. S. is supported by Leverhulme Trust Grant No. RPG-2019-350, European Union's H2020 ERC Starting Grant No. 945155–GWmining, and Cariplo Foundation Grant No. 2021-0555. P. S. acknowledges support from STFC Grant No. ST/V005677/1. A. V. acknowledges the support of the Royal Society and Wolfson Foundation. Computational resources used for this work were provided by the University of Birmingham's BlueBEAR High Performance Computing facility and the Bondi HPC Cluster at the Birmingham Institute for Gravitational Wave Astronomy.

APPENDIX: POSTERIOR DISTRIBUTIONS

Here we provide full corner plots of the posterior probability density functions on the system parameters for the runs listed in Table I and discussed in the main text. For the sake of readability, we omit the coalescence phase and the polarization, which do not carry important physical information about the binaries.

[1] M. Volonteri, Astron. Astrophys. Rev. **18**, 279 (2010).
[2] P. Amaro-Seoane *et al.* (LISA Collaboration), arXiv:1702.00786.
[3] P. Amaro-Seoane *et al.*, Living Rev. Relativity **26**, 2 (2023).
[4] Ž. Ivezić *et al.* (LSST Collaboration), Astrophys. J. **873**, 111 (2019).
[5] A. Wootten and A. R. Thompson, IEEE Proc. **97**, 1463 (2009).
[6] P. E. Dewdney, P. J. Hall, R. T. Schilizzi, and T. J. L. W. Lazio, IEEE Proc. **97**, 1482 (2009).
[7] J. P. Gardner *et al.*, Space Sci. Rev. **123**, 485 (2006).
[8] K. Nandra *et al.*, arXiv:1306.2307.
[9] A. Sesana, Front. Astron. Space Sci. **8**, 7 (2021).
[10] P. Madau and M. J. Rees, Astrophys. J. Lett. **551**, L27 (2001).
[11] T. H. Greif, V. Springel, S. D. M. White, S. C. O. Glover, P. C. Clark, R. J. Smith, R. S. Klessen, and V. Bromm, Astrophys. J. **737**, 75 (2011).
[12] A. Klein *et al.*, Phys. Rev. D **93**, 024003 (2016).
[13] M. C. Begelman, M. Volonteri, and M. J. Rees, Mon. Not. R. Astron. Soc. **370**, 289 (2006).
[14] M. Volonteri, G. Lodato, and P. Natarajan, Mon. Not. R. Astron. Soc. **383**, 1079 (2008).
[15] A. E. Reines and M. Volonteri, Astrophys. J. **813**, 82 (2015).
[16] Á. Bogdán, L. Lovisari, M. Volonteri, and Y. Dubois, Astrophys. J. **852**, 131 (2018).
[17] D. Baron and B. Ménard, Mon. Not. R. Astron. Soc. **487**, 3404 (2019).
[18] LISA Science Study Team, LISA science requirements document, 1.0, Technical Report No. ESA-L3-EST-SCI-RS-001, European Space Agency, 2018.
[19] S. Babak, M. Hewitson, and A. Petiteau, arXiv:2108.01167.
[20] K. G. Arun *et al.*, Classical Quantum Gravity **26**, 094027 (2009).
[21] A. Mangiagli, A. Klein, M. Bonetti, M. L. Katz, A. Sesana, M. Volonteri, M. Colpi, S. Marsat, and S. Babak, Phys. Rev. D **102**, 084056 (2020).

[22] S. Marsat, J. G. Baker, and T. D. Canton, Phys. Rev. D **103**, 083011 (2021).
[23] V. Baibhav, E. Berti, and V. Cardoso, Phys. Rev. D **101**, 084053 (2020).
[24] M. L. Katz, Phys. Rev. D **105**, 044055 (2022).
[25] A. Mangiagli, C. Caprini, M. Volonteri, S. Marsat, S. Vergani, N. Tamanini, and H. Inchauspé, Phys. Rev. D **106**, 103017 (2022).
[26] R. Wang and B. Hu, arXiv:2208.13351.
[27] C. Cutler and É. E. Flanagan, Phys. Rev. D **49**, 2658 (1994).
[28] V. Varma, P. Ajith, S. Husa, J. C. Bustillo, M. Hannam, and M. Pürrer, Phys. Rev. D **90**, 124004 (2014).
[29] V. Varma and P. Ajith, Phys. Rev. D **96**, 124024 (2017).
[30] K. Chatziioannou *et al.*, Phys. Rev. D **100**, 104015 (2019).
[31] F. H. Shaik, J. Lange, S. E. Field, R. O'Shaughnessy, V. Varma, L. E. Kidder, H. P. Pfeiffer, and D. Wysocki, Phys. Rev. D **101**, 124054 (2020).
[32] R. Abbott *et al.* (LIGO Scientific and Virgo Collaborations), Phys. Rev. D **102**, 043015 (2020).
[33] T. A. Prince, M. Tinto, S. L. Larson, and J. W. Armstrong, Phys. Rev. D **66**, 122002 (2002).
[34] L. J. Rubbo, N. J. Cornish, and O. Poujade, Phys. Rev. D **69**, 082003 (2004).
[35] S. Babak, J. Gair, A. Sesana, E. Barausse, C. F. Sopuerta, C. P. L. Berry, E. Berti, P. Amaro-Seoane, A. Petiteau, and A. Klein, Phys. Rev. D **95**, 103012 (2017).
[36] P. C. Peters, Phys. Rev. **136**, B1224 (1964).
[37] G. Pratten, S. Husa, C. Garcia-Quiros, M. Colleoni, A. Ramos-Buades, H. Estelles, and R. Jaume, Phys. Rev. D **102**, 064001 (2020).
[38] C. García-Quirós, M. Colleoni, S. Husa, H. Estellés, G. Pratten, A. Ramos-Buades, M. Mateu-Lucena, and R. Jaume, Phys. Rev. D **102**, 064002 (2020).
[39] N. Aghanim *et al.* (Planck Collaboration), Astron. Astrophys. **641**, A6 (2020); **652**, C4(E) (2021).
[40] E. Roebber *et al.*, Astrophys. J. Lett. **894**, L15 (2020).
[41] R. Buscicchio, A. Klein, E. Roebber, C. J. Moore, D. Gerosa, E. Finch, and A. Vecchio, Phys. Rev. D **104**, 044065 (2021).
[42] A. Klein *et al.*, arXiv:2204.03423.
[43] E. Finch *et al.*, Mon. Not. R. Astron. Soc. **522**, 5358 (2023).
[44] J. Skilling, AIP Conf. Proc. **735**, 395 (2004).
[45] J. S. Speagle, Mon. Not. R. Astron. Soc. **493**, 3132 (2020).
[46] E. Barausse, Mon. Not. R. Astron. Soc. **423**, 2533 (2012).
[47] T. Damour, Phys. Rev. D **64**, 124013 (2001).
[48] E. Racine, Phys. Rev. D **78**, 044021 (2008).
[49] P. Ajith *et al.*, Phys. Rev. Lett. **106**, 241101 (2011).
[50] S. Vitale, R. Lynch, J. Veitch, V. Raymond, and R. Sturani, Phys. Rev. Lett. **112**, 251101 (2014).
[51] M. Pürrer, M. Hannam, and F. Ohme, Phys. Rev. D **93**, 084042 (2016).
[52] S. Vitale, R. Lynch, V. Raymond, R. Sturani, J. Veitch, and P. Graff, Phys. Rev. D **95**, 064053 (2017).
[53] G. Pratten, P. Schmidt, R. Buscicchio, and L. M. Thomas, Phys. Rev. Res. **2**, 043096 (2020).
[54] N. V. Krishnendu and F. Ohme, Phys. Rev. D **105**, 064012 (2022).
[55] S. McGee, A. Sesana, and A. Vecchio, Nat. Astron. **4**, 26 (2020).
[56] C. Palenzuela, L. Lehner, and S. L. Liebling, Science **329**, 927 (2010).
[57] E. M. Rossi, G. Lodato, P. J. Armitage, J. E. Pringle, and A. R. King, Mon. Not. R. Astron. Soc. **401**, 2021 (2010).
[58] L. M. Krauth, J. Davelaar, Z. Haiman, J. R. Westernacher-Schneider, J. Zrake, and A. MacFadyen, arXiv:2304.02575.
[59] S. Nissanke, D. E. Holz, S. A. Hughes, N. Dalal, and J. L. Sievers, Astrophys. J. **725**, 496 (2010).
[60] B. F. Schutz, Classical Quantum Gravity **28**, 125023 (2011).
[61] B. P. Abbott *et al.* (LIGO Scientific and Virgo Collaborations), Phys. Rev. Lett. **119**, 161101 (2017).
[62] H.-Y. Chen, S. Vitale, and R. Narayan, Phys. Rev. X **9**, 031028 (2019).
[63] S. A. Usman, J. C. Mills, and S. Fairhurst, Astrophys. J. **877**, 82 (2019).
[64] L. P. Singer and L. R. Price, Phys. Rev. D **93**, 024013 (2016).
[65] L. P. Singer *et al.*, Astrophys. J. Lett. **829**, L15 (2016).
[66] LIGO.SKYMAP, https://lscsoft.docs.ligo.org/ligo.skymap/.
[67] M. L. Katz, S. Marsat, A. J. K. Chua, S. Babak, and S. L. Larson, Phys. Rev. D **102**, 023033 (2020).
[68] T. Bogdanović, C. S. Reynolds, and M. C. Miller, Astrophys. J. Lett. **661**, L147 (2007).
[69] N. Steinle and D. Gerosa, Mon. Not. R. Astron. Soc. **519**, 5031 (2023).
[70] T. A. Apostolatos, C. Cutler, G. J. Sussman, and K. S. Thorne, Phys. Rev. D **49**, 6274 (1994).
[71] P. Schmidt, M. Hannam, and S. Husa, Phys. Rev. D **86**, 104063 (2012).
[72] A. Vecchio, Phys. Rev. D **70**, 042001 (2004).
[73] R. N. Lang and S. A. Hughes, Phys. Rev. D **74**, 122001 (2006).
[74] Q. Baghi, I. Thorpe, J. Slutsky, J. Baker, T. Dal Canton, N. Korsakova, and N. Karnesis, Phys. Rev. D **100**, 022003 (2019).
[75] K. Dey, N. Karnesis, A. Toubiana, E. Barausse, N. Korsakova, Q. Baghi, and S. Basak, Phys. Rev. D **104**, 044035 (2021).
[76] M. C. Edwards, P. Maturana-Russel, R. Meyer, J. Gair, N. Korsakova, and N. Christensen, Phys. Rev. D **102**, 084062 (2020).